Available online at www.sciencedirect.com
ScienceDirect
Ceramics International 36 (2010) 661–672
CERAMICS INTERNATIONAL
www.elsevier.com/locate/ceramint

# Synthesis of monoclinic Celsian from Coal Fly Ash by using a one-step solid-state reaction process

D. Long-González [a], J. López-Cuevas [a,*], C.A. Gutiérrez-Chavarría [a], P. Pena [b], C. Baudin [b], X. Turrillas [c]

[a] CINVESTAV-IPN, Unidad Saltillo, Carretera Saltillo-Monterrey, Km. 13.5, 25900, Ramos Arizpe, Coahuila, Mexico
[b] Instituto de Cerámica y Vidrio, CSIC, Kelsen 5, E-28049 Madrid, Spain
[c] Eduardo Torroja Institute for Construction Sciences, CSIC, Serrano Galvache 4, E-28033 Madrid, Spain

Received 20 February 2009; received in revised form 2 March 2009; accepted 30 September 2009
Available online 5 November 2009

**Abstract**

Monoclinic (Celsian) and hexagonal (Hexacelsian) $Ba_{1-x}Sr_xAl_2Si_2O_8$ solid solutions, where $x = 0, 0.25, 0.375, 0.5, 0.75$ or 1, were synthesized by using Coal Fly Ash (CFA) as main raw material, employing a simple one-step solid-state reaction process involving thermal treatment for 5 h at 850–1300 °C. Fully monoclinic Celsian was obtained at 1200 °C/5 h, for SrO contents of $0.25 \leq x \leq 0.75$. However, an optimum SrO level of $0.25 \leq x \leq 0.375$ was recommended for the stabilization of Celsian. These synthesis conditions represent a significant improvement over the higher temperatures, longer times and/or multi-step processes needed to obtain fully monoclinic Celsian, when other raw materials are used for this purpose, according to previous literature. These results were attributed to the role of the chemical and phase constitution of CFA as well as to a likely mineralizing effect of CaO and $TiO_2$ present in it, which enhanced the Hexacelsian to Celsian conversion.
© 2009 Elsevier Ltd and Techna Group S.r.l. All rights reserved.

*Keywords:* (A) Powders: solid-state reaction; (B) X-ray methods; (E) Thermal applications; Celsian

## 1. Introduction

Due to its high resistance to oxidation and reduction [1], low dielectric constant [2] and low thermal expansion coefficient [3], barium aluminosilicate ($BaAl_2Si_2O_8$, or $BAS_2$)[1], particularly in its monoclinic form, constitutes an attractive material for the matrix of ceramic composites [4,5], as well as for protective coatings [6]. $BaAl_2Si_2O_8$ has three polymorphic forms: monoclinic (usually denominated either as Celsian or as Monocelsian), hexagonal (Hexacelsian) and orthorhombic [3,7]. The melting point of stoichiometric $BaAl_2Si_2O_8$ is 1760 °C. Hexacelsian is the stable phase between 1590 and 1760 °C, and Celsian is stable below 1590 °C. However, Hexacelsian may exist metastably below the latter temperature due to a sluggish hexagonal to monoclinic conversion [8]. Hexacelsian is an undesirable phase due to its high mean thermal expansion coefficient of $8 \times 10^{-6}$/°C (300–1000 °C) [3,9], when compared to the value of $2.26 \times 10^{-6}$/°C (20–1000 °C) reported for Celsian [3,10]. Besides, Hexacelsian transforms into the orthorhombic form at 300 °C, which is accompanied by a volume change of ~3–4%, with a consequent microcracking of the material. Thus, successful employment of $BaAl_2Si_2O_8$ requires a previous stabilization of its monoclinic form. It is well-known that the hexagonal to monoclinic conversion is greatly enhanced by the addition of mineralizers such as $Li_2O$, MgO, CaO, NaF and $TiO_2$ [11,12]. On the other hand, I.G. Talmy and D.A. Haught, as quoted by Bansal et al. [13], showed that partial substitution of BaO by SrO in polycrystalline $BaAl_2Si_2O_8$ facilitates the Hexacelsian to Celsian transformation and, under certain conditions, Hexacelsian may never form.

Generally $BaAl_2Si_2O_8$ is synthesized from stoichiometric mixtures of $Al_2O_3$, $SiO_2$ and $BaCO_3$ reagent-grade powders.

* Corresponding author. Tel.: +52 844 4389600; fax: +52 844 4389610.
*E-mail address:* jorge.lopez@cinvestav.edu.mx (J. López-Cuevas).

[1] For simplicity, solid phases given in the figures and tables of this paper are described by abbreviated formulas: C = CaO, B = BaO, $SiO_2$ = S, SrO = s, and A = $Al_2O_3$ (i.e., $BaAl_2O_4$ = BaO·$Al_2O_3$ = BA; $BaSiO_3$ = BaO·$SiO_2$ = BS; $Ba_2SiO_4$ = 2BaO·$SiO_2$ = $B_2S$; $BaSi_2O_5$ = BaO·2$SiO_2$ = $BS_2$; $Sr_2SiO_4$ = 2SrO·$SiO_2$ = $s_2S$; $SrSiO_3$ = SrO·$SiO_2$ = sS; $SrAl_2O_4$ = SrO·$Al_2O_3$ = sA; $BaAl_2Si_2O_8$ = BaO·$Al_2O_3$·2$SiO_2$ = $BAS_2$ and $Sr_2Al_2SiO_7$ = $s_2AS$).

0272-8842/$36.00 © 2009 Elsevier Ltd and Techna Group S.r.l. All rights reserved.
doi:10.1016/j.ceramint.2009.10.008

However, a variety of other alternative raw materials can also be used for this purpose, among which Coal Fly Ash (CFA) is one of the less frequently employed [14]. CFA is a byproduct of coal-burning power plants, whose main chemical constituents are $SiO_2$ and $Al_2O_3$, and whose main mineralogical components are quartz, mullite ($Al_6Si_2O_{13}$) and a highly reactive amorphous phase [15]. Millions of Tons of CFA are produced all over the world each year, most of which are discarded, with minimum use mainly as additive for Portland cement. As a result, an abundant and cheap potential source of $SiO_2$ and $Al_2O_3$, which is already fine and which does not require to be extracted or mined, is basically wasted.

Thus, this work was focused on the synthesis of Celsian, with and without SrO doping, using CFA as main raw material, with particular attention given to the reaction mechanism, as well as to a likely mineralizing effect of impurities contained in the CFA on stabilization of the monoclinic phase. It is worth mentioning that Amritphale et al. [14], who are up to now the only researchers to have used CFA as raw material for the synthesis of Celsian $BaAl_2Si_2O_8$-containing ceramics, did not study either the Hexacelsian to Celsian transformation or the effect of SrO doping on the latter transformation in their materials. In fact, the chemical compositions studied by these authors differ greatly from those studied in the present work, in such a way that completely different phase compositions and microstructures were obtained in both cases, and for different intended applications.

A further objective of this work was to develop a relatively low-temperature solid-state synthesis process which was simpler and of shorter duration than those recommended in previous literature reports [16] for the production of Celsian.

## 2. Experimental procedure

$Ba_{1-x}Sr_xAl_2Si_2O_8$ solid solutions, where $x = 0$, 0.25, 0.375, 0.5, 0.75 or 1, were synthesized by using a simple one-step solid-state reaction process, employing suitable mixtures of Coal Fly Ash (CFA), $BaCO_3$ (purity of 99.43 wt.%, Alkem, México), $SrCO_3$ (purity of 97.86 wt.%, Solvay, México) and $Al_2O_3$ (HPA-0.5, purity of 99.99 wt.%, Sasol, USA). Monoclinic and hexagonal solid solutions, with SrO contents in the range of $0.25 \leq x \leq 0.75$, are hereinafter denominated as Celsian and Hexacelsian, respectively. The limiting compositions with monoclinic structure are denominated as Ba-Celsian $BaAl_2Si_2O_8$, for $x = 0$, and Sr-Celsian $SrAl_2Si_2O_8$, for $x = 1$.

CFA was collected directly from the cyclone precipitators of ''José López Portillo'' power plant located in the city of Nava, Coahuila, México. Then, the CFA was beneficiated in order to eliminate as much $Fe_2O_3$ as possible. For this, the CFA was first sieved using a 125 μm mesh. Then, the sieved CFA was ball milled for 5 h in order to liberate the $Fe_2O_3$ embedded in some of the CFA particles. Subsequently, the milled material was subjected to manual wet magnetic separation using a powerful neodymium magnet. The CFA was analyzed by X-ray fluorescence (Bruker AXS S4 Pioneer XRF, Saltillo, México), X-ray diffraction (Philips X'PERT XRD 3040, $CuK_\alpha$ radiation, Saltillo, México), scanning electron microscopy (Philips XL30 ESEM, Saltillo, México) and simultaneous thermogravimetric and differential thermal analyses TGA/DTA (Perkin Elmer Pyris Diamond 7 apparatus, Pt crucibles and heating rate of 10 °C/min, Saltillo, México), before and after magnetic separation. The mean particle size of all raw materials was determined by laser diffraction (Coulter LS-100 particle size analyzer, Saltillo, México), see Table 1.

Table 1
Mean particle size of raw materials.

| Raw materials | Particle size (μm) |
|---|---|
| CFA | 63 (as-received), 5 (after ball milling) |
| $Al_2O_3$ | <1 |
| $BaCO_3$ | 3 |
| $SrCO_3$ | 4 |

The raw materials were mixed in a two-station Retsch PM-200 planetary mill (Saltillo, México) for 1 h at 350 rpm, using agate balls and mortars, and a powder to balls ratio of 1:2. The proportions of CFA, $Al_2O_3$, $BaCO_3$ and $SrCO_3$ in the green powder mixtures prepared are shown in Table 2.

All green powder mixtures were uniaxially pressed at 95 MPa in order to obtain disks with a diameter of 12 mm and thickness of 5 mm. These disks were subsequently thermally treated for 5 h in a Thermolyne 46200 high temperature furnace, in the temperature range of 850–1300 °C, using a heating rate of 5 °C/min. After the thermal treatment, the furnace was cooled down to room temperature at a cooling rate of 5 °C/min. A non-compacted and non-thermally treated powder sample was subjected to simultaneous TGA/DTA studies, under the same conditions used for the CFA, in order to determine the decomposition temperature of carbonates. A cross-section of all thermally treated samples was cut off with diamond saw and flatten out on a lapping plate using 40 μm diamond particles, followed by successive grinding steps using 1200 and 2500 SiC grit sizes. A final polish was then given to all samples in successive steps using 6, 3 and 1 μm diamond

Table 2
Composition of green powder mixtures (wt.%) with expected crystalline $Ba_{1-x}Sr_xAl_2Si_2O_8$ after heat treatment.

| *X* | Sample code | CFA | $Al_2O_3$ | $BaCO_3$ | $SrCO_3$ |
|---|---|---|---|---|---|
| 0 | $BAS_2$ | 42.62 | 13.40 | 44.07 | – |
| 0.25 | B7S2 | 43.78 | 13.76 | 33.99 | 8.46 |
| 0.375 | B6S3 | 44.42 | 13.97 | 28.72 | 12.89 |
| 0.5 | B5S5 | 45.07 | 14.17 | 23.31 | 17.44 |
| 0.75 | B2S7 | 46.44 | 14.60 | 12.00 | 26.95 |
| 1.0 | SAS | 47.87 | 15.07 | – | 37.06 |

Table 3
Parameters of the departure model used for the refinements. Space Group *C2/m* (no. 12). Cell parameters $a = 8.633(6)$ Å, $b = 13.063(8)$ Å, $c = 7.214(5)$ Å, $\beta = 115.17(5)^\circ$.

| Name | Mult. | Wyckoff | *x* | *y* | *z* | Uiso | Occ. | Species |
|---|---|---|---|---|---|---|---|---|
| Ba | 4 | (i) | 0.28270 | 0.0000 | 0.13057 | 0.0203 | 0.938 | Ba |
| T1 | 8 | (j) | 0.00832 | 0.18272 | 0.22450 | 0.0167 | 1.00 | Si/Al |
| T2 | 8 | (j) | 0.20313 | 0.38148 | 0.34697 | 0.0165 | 1.00 | Si/Al |
| O1 | 4 | (g) | 0.0000 | 0.1381 | 0.00000 | 0.0192 | 1.00 | O |
| O2 | 4 | (i) | 0.1209 | 0.5000 | 0.28780 | 0.0220 | 1.00 | O |
| O3 | 8 | (j) | 0.3266 | 0.3626 | 0.22410 | 0.0259 | 1.00 | O |
| O4 | 8 | (j) | 0.0251 | 0.3101 | 0.25200 | 0.0250 | 1.00 | O |
| O5 | 8 | (j) | 0.1865 | 0.1264 | 0.39700 | 0.0245 | 1.00 | O |

Table 4
Chemical analysis of CFA (wt.%).

| CFA | $SiO_2$ | $Al_2O_3$ | $Fe_2O_3$ | CaO | MgO | $Na_2O$ | $K_2O$ | $TiO_2$ | Other oxides[a] | LOI |
|---|---|---|---|---|---|---|---|---|---|---|
| As-received | 60.33 | 24.93 | 7.13 | 1.97 | 0.52 | 0.59 | 0.69 | 0.60 | 0.85 | 2.38 |
| Beneficiated | 64.59 | 25.73 | 2.57 | 2.12 | 0.48 | 0.46 | 0.37 | 0.59 | 1.11 | 1.94 |

[a] SrO, $ZrO_2$, CuO, NiO, $SO_3$ and $P_2O_5$.

particles on a medium nap cloth. Then the gold-coated surfaces of the samples were examined by SEM, with and without chemical etching (5 s in a 5 vol.% HF aqueous solution). These samples were also analyzed by XRD after manual grinding using Diamonite mortar and pestle, until a final particle size of ~125 μm was achieved. XRD was also used in order to determine a semi-quantitative Hexacelsian to Celsian conversion fraction ($f$, %), by using the following expression [17]:

$$f = \frac{I_{\text{mono}}}{I_{\text{mono}} + I_{\text{hexa}}} \times 100$$

where $I_{\text{hexa}}$ and $I_{\text{mono}}$ are the integrated intensities for the (1 0 1) reflection of Hexacelsian and for the (1 3 0) reflection of Celsian, respectively. JCPDS-files were used to analyze the XRD spectra.

In order to determine the cell parameters and populations of large cations in the synthesized materials, their XRD patterns were fitted by the Pawley and Rietveld methods. For this, a Siemens D5000 XRD apparatus (Karlsruhe, Germany), equipped with a copper target X-ray tube, was used. The slits used were: divergence, 2 mm wide, receiving, 0.2 mm, and detector, 0.6 mm. Diffraction patterns were collected between 10° and 70° (2$\theta$) in steps of 0.02° (2$\theta$), counting for 16 s while specimens were rotated at 15 rpm. The Materials Studio 4 (MS4) software package [18] was used for the refinements. The crystal model used as an initial guess was the one published by Skellern et al. [19], see Table 3. The powders to be analyzed were ground in an agate mortar, placed over a flat glass surface, and uniformly distributed over the surface with the help of a steel blade to diminish preferential orientations. Finally, the glass sample holder covered with a thin film of Vaseline was turned over the flat glass surface containing the powders to get a uniform coat of specimen adhered to the sample holder. Neither the glass sample holder nor the Vaseline used produced any diffraction signals.

To back up the reaction mechanism proposed, free energy computations for all possible reactions between BaO, $SiO_2$, SrO and $Al_2O_3$ were performed using HSC [20]. This is a computing package that offers an exhaustive thermochemical database and includes enthalpy (H), entropy (S) and heat capacity (C) data for chemical compounds.

## 3. Results and discussion

### 3.1. Characterization of CFA

The chemical compositions of as-received and beneficiated CFA are given in Table 4. In both cases, $SiO_2$ and $Al_2O_3$ are the main components of CFA, while its main impurities are $Fe_2O_3$ and CaO. The combined $SiO_2 + Al_2O_3$ content increased from 85.3 to 90.3 wt.% after the beneficiation process. However, while the $Fe_2O_3$ content was reduced in 64.4 wt.% after this process,

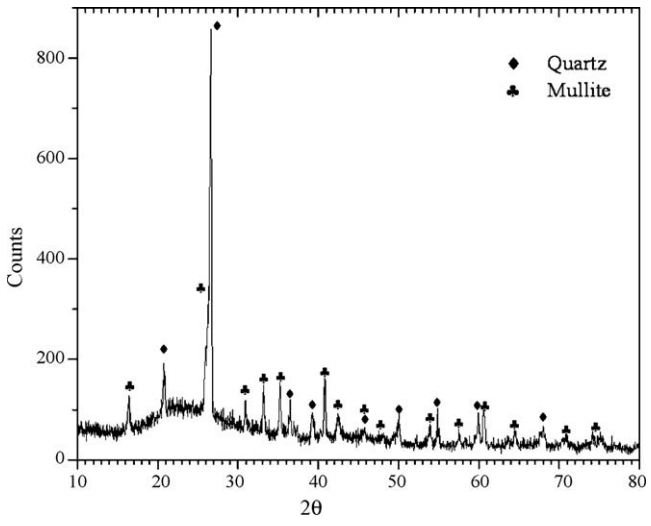


Fig. 1. XRD pattern of beneficiated CFA.

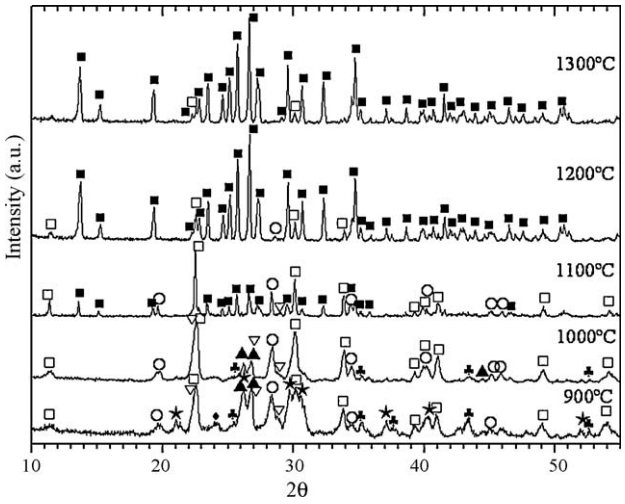


Fig. 2. XRD powder patterns of $BAS_2$ nominal composition, heat treated at different temperatures for 5 h. Crystalline phases detected: C (■), H (□), A (♣), BA (○), BS (▲), $B_2S$ (★), $BS_2$ (▽), and W (◆).

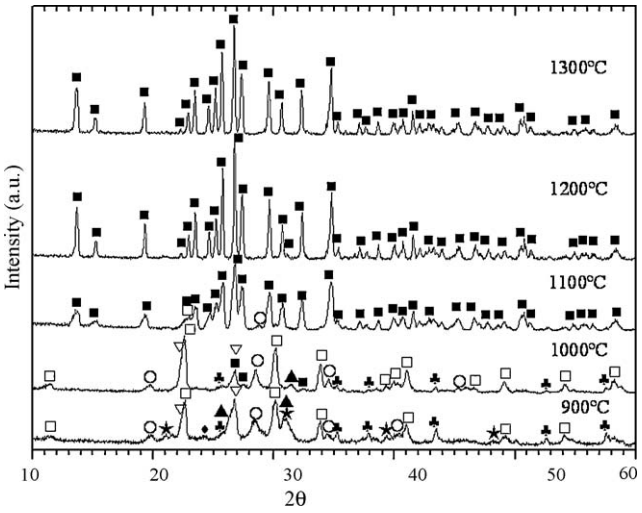


Fig. 3. XRD powder patterns of B7S2 nominal composition, heat treated at different temperatures for 5 h. Crystalline phases detected: C (■), H (□), A (♣), BA (○), BS (▲), $B_2S$ (★), $BS_2$ (▽), and W (◆).

that of CaO remained relatively unchanged in a level close to 2 wt.%. The Loss On Ignition (LOI) of ∼2 wt.% corresponded basically to free carbon present in the CFA, whose level was only slightly reduced by the beneficiation process.

Fig. 1 shows the XRD pattern of beneficiated CFA. Only quartz and mullite crystalline phases plus a large proportion of amorphous phase were detected. Amorphous phase is visible in the intense broad background (centre: *ca.* 23°, 2$\theta$), which is a characteristic feature of this phase.

Dissolution of CFA with HF acid [21,22], followed by ICP chemical analysis of the resulting solution, allowed us to estimate that CFA contains ∼75 wt.% of amorphous phase, with a chemical composition of 74 wt.% $SiO_2$ and 18 wt.% $Al_2O_3$ (balance corresponding to $Fe_2O_3$, CaO, plus other minor impurities). These calculations were carried out assuming that the impurities were basically contained in the glassy phase. Impurities such as $Fe_2O_3$, remaining in the CFA after the beneficiation process, were not detected by XRD because a part of them was present as crystalline phases with a level below the detection limit of the technique employed, while another part was contained in the amorphous phase, also in a low level.

SEM analysis showed that the as-received CFA was composed predominantly by small spherical particles, which were either solid or hollow (cenospheres and plenospheres). Some flake-like particles were also observed.

### 3.2. Characterization of heat-treated samples

The chemical analyses of heat-treated materials are shown in Table 5. Calculated compositions are given inside the parentheses. Small differences observed between the calculated and the analyzed compositions can be attributed to small errors in sample preparation and chemical analysis, as well as to the presence of impurities in the CFA. However, in all cases the analyzed $SiO_2/Al_2O_3$ and $SiO_2$/BaO weight ratios were very close to the theoretical ones.

The phase evolution of the $BAS_2$ and B7S2 nominal compositions as a function of temperature can be followed from the XRD patterns shown in Figs. 2 and 3, respectively. The $BAS_2$ material was fully transformed into $BaAl_2Si_2O_8$, mainly in its monoclinic form, after thermally treated at 1300 °C/5 h. On the other hand, the B7S2 nominal composition, Fig. 3, achieved full transformation into monoclinic Celsian at 1200 °C/5 h. The same result was obtained for the B6S3 and B5S5 nominal compositions, according to Table 6, which gives a summary of the XRD results obtained for all nominal compositions and temperatures studied. In contrast, the B2S7 and SAS nominal compositions achieved a full transformation into monoclinic Celsian at 1300 °C/5 h, with the presence of traces of Hexacelsian and strontium aluminate in SAS.

These results indicate that both undoped and SrO-doped monoclinic Celsian can be obtained at relatively low

Table 5
Analyzed chemical composition (wt.%) of materials with nominal composition of $Ba_{1-x}Sr_xAl_2Si_2O_8$, after heat treatment at 1200 °C/5 h.

| *X* | Sample code | $SiO_2$ | $Al_2O_3$ | BaO | SrO | $Fe_2O_3$ | CaO | MgO | $Na_2O$ | $K_2O$ | $TiO_2$ | Other oxides |
|---|---|---|---|---|---|---|---|---|---|---|---|---|
| 0 | $BAS_2$ | 30.46 | 25.85 | 38.87 | 0.32 | 1.25 | 1.31 | 0.18 | 0.38 | 0.55 | 0.55 | 0.26 |
| 0.25 | B7S2 | 31.49 | 26.72 | 30.13 | 6.79 | 1.40 | 1.46 | 0.18 | 0.29 | 0.65 | 0.60 | 0.26 |
| 0.375 | B6S3 | 32.52 | 27.02 | 25.39 | 10.30 | 1.61 | 1.62 | 0.23 | 0.35 | 0.77 | 0.60 | 0.20 |
| 0.5 | B5S5 | 32.48 | 27.55 | 20.72 | 14.00 | 1.61 | 1.55 | 0.26 | 0.38 | 0.68 | 0.58 | 0.15 |
| 0.75 | B2S7 | 33.38 | 28.31 | 10.65 | 21.58 | 2.25 | 1.62 | 0.31 | 0.36 | 0.75 | 0.61 | 0.16 |
| 1.0 | SAS | 34.89 | 29.61 | 0.83 | 30.10 | 1.34 | 1.50 | 0.23 | 0.22 | 0.69 | 0.45 | 0.10 |

Table 6
Summary of results of XRD analyses of thermally treated samples[a].

| Treatment temperature (°C) | $BAS_2$ | B7S2 | B6S3 | B5S5 | B2S7 | SAS |
|---|---|---|---|---|---|---|
| 850 | A,W,$B_2S$,BS, $BS_2$, H | A,$B_2S$,$BS_2$, W,BS,H | *** | *** | *** | R,A,M,$S_2S$ |
| 900 | H,A,BA,BS, $B_2S$,$BS_2$,$W^t$ | H,A,$B_2S$, $BS_2$,BA,BS,$W^t$ | H,A,BA, $BS_2$,BS | H,A,$BS_2$, $B_2S$,BA,$BS^t$ | H,A,$S_2S$,SS, $SA^t$ | A,$S_2S$,H,SS, SA,$S_2AS$ |
| 1000 | H,BA,$BS_2$,A | H,A,BA, $BS_2$,C,$BS^t$ | H,A,C, $BS_2$,BA, BS | H,C,A,BA, $BS_2$,$B_2S$ | H,C,A,$S_2S$, SA,SS | SS,$S_2S$,A,H, SA,$S_2AS$ |
| 1100 | H,C,BA,$BS_2{}^t$ | C,$BA^t$,$H^t$ | C,$H^t$,$BA^t$ | C,$H^t$,$BA^t$ | C,SS,$H^t$,$SA^t$ | C,SS,A,SA,H, $S_2AS$,$S_2S^t$ |
| 1200 | C,H,$BA^t$ | C | C | C | C,$SA^t$ | C,SA,$S_2AS^t$,$H^t$ |
| 1300 | C,H | C | C | C | C | C,$H^t$,$SA^t$ |

[a] Notation used in Figs. 2 and 3, and Table 6, is: Celsian (C), Hexacelsian (H), $Al_2O_3$ (A), $BaAl_2O_4$ (BA), $BaSiO_3$ (BS), $Ba_2SiO_4$ ($B_2S$), $BaSi_2O_5$ ($BS_2$), $BaCO_3$ (W), $Sr_2SiO_4$ ($s_2S$), $SrSiO_3$ (sS), $SrAl_2O_4$ (sA), $Sr_2Al_2SiO_7$ ($s_2AS$), $Al_6Si_2O_{13}$ (M), and $SrCO_3$ (R).
*** Not analyzed. t = trace.

temperatures and short thermal treatments using a simple one-step process when CFA is employed as the main raw material. In general, doping the $BaAl_2Si_2O_8$ composition with SrO in the range of $0.25 \leq x \leq 0.75$, resulted in a reduction of 100 °C in the temperature required for full transformation of Hexacelsian into Celsian. These synthesis conditions represent a significant improvement over the higher temperatures, longer times and/or multi-step processes needed for full conversion when other raw materials (either amorphous or crystalline, and either mineral or reagent-grade) are used for the synthesis of $BaAl_2Si_2O_8$, with or without SrO doping, according to previously published literature, as described below.

Regarding the synthesis of Celsian $BaAl_2Si_2O_8$ without SrO doping, Moya Corral and Verduch [3] obtained this phase by solid-state reaction of mixtures of kaolin and $BaCO_3$ at 1350 °C/24 h. Talmy and Haught [23] synthesized the same phase from $BaCO_3$, $Al_2O_3$ and amorphous $SiO_2$ at 1500 °C for ~150 h. Bansal et al. [13] obtained full monoclinic $BaAl_2Si_2O_8$ from cold isostatically pressed and sintered (1300 °C/20 h) glass powders. Lastly, Lee and Aswath [16] synthesized Celsian $BaAl_2Si_2O_8$ using a three-step process, with or without the addition of $Li_2O$. In the first step, $SiO_2$ and $BaCO_3$ were reacted at 1150 °C/4 h in order to form barium silicate, avoiding in this way the formation of barium aluminate, which is much less reactive than barium silicate and, thus, delays the formation of Celsian. In the second step, barium silicate was reacted with $Al_2O_3$ at 1200 °C/6 h in order to form Hexacelsian. In the third step, Hexacelsian was ground, encouraging in this way the formation of monoclinic Celsian nucleus, and then heat treated at 1200–1530 °C for 4–50 h, in order to promote its conversion into Celsian. Pure Celsian was obtained when ground pre-synthesized Hexacelsian was doped with 0.4 wt.% $Li_2O$, followed by thermal treatment at 900 °C/4 h.

Regarding the use of SrO doping for the synthesis of monoclinic $Ba_{1-x}Sr_xAl_2Si_2O_8$, Fu et al. [17] obtained this phase by solid-state reaction of mixtures of $BaCO_3$, $SrCO_3$, $Al_2O_3$ and $SiO_2$ reagent-grade powders, observing an increase in the Hexacelsian to Celsian conversion with increasing SrO content, achieving a maximum conversion of ~40% for $x = 0.375$ after calcination at 950 °C/4 h, which was followed by heat treatment at 1040 °C/4 h. Bansal [24] obtained Celsian with chemical composition of $Ba_{0.75}Sr_{0.25}Al_2Si_2O_8$ by solid-state reaction of a suitable mixture of $Al_2O_3$, $SiO_2$, $BaCO_3$ and $SrCO_3$ reagent-grade powders, which was first calcined at ~900–910 °C for 24 h and then ground, following this by hot pressing at 1300 °C for 2–3 h under a pressure of 27.5 MPa. Krzmanc et al. [25] synthesized a material with the same composition by solid-state reaction at 1100 °C/12 h, using similar raw materials, obtaining a mixture of Hexacelsian and Monocelsian, in which the first phase predominated. Bansal [26], on the other hand, was able to achieve full conversion of Hexacelsian into Celsian for a monolithic specimen containing 90 wt.% $BaAl_2Si_2O_8$ glass and 10 wt.% $SrAl_2Si_2O_8$ glass, either after hot pressing at 1000 °C for 10 min at 13.8 MPa, followed by annealing at 1200 °C/2 h, or after hot pressing at 1300 °C/2 h under 13.8 MPa. Lastly, Bansal et al. [13] obtained full monoclinic Celsian from cold isostatically pressed and sintered (above 900 °C for 20 h) $BaAl_2Si_2O_8$ glass powders doped either with 9.87 or with 18.6 wt.% SrO. In Refs. [13,26], the initial glasses were obtained by melting suitable mixtures of $BaCO_3$, $SrCO_3$, $Al_2O_3$ and $SiO_2$ reagent-grade powders at temperatures of ~2000–2100 °C.

As for the case of undoped and SrO-doped $BaAl_2Si_2O_8$ compositions, the conditions employed in this work for the synthesis of Celsian SAS represent also a significant improvement over the higher temperatures, longer times and/or multi-step processes needed for full conversion of Hexacelsian into Celsian, according to previous literature reports. For instance, Kobayashi and Inagaki [27] obtained full monoclinic Celsian SAS by solid-state reaction of stoichiometric mixtures of kaolin and $SrCO_3$, which were calcined at 800 °C for several hours, then milled for 1–20 h and uniaxially pressed at 98 MPa, following this by heat treatment at 1200 °C/1 h. On the other hand, Bansal et al. [13] obtained full monoclinic Celsian SAS from cold isostatically pressed and sintered (1100 °C/20 h) glass powders.

### 3.3. Reaction mechanism for the formation of Celsian

In order to obtain additional information regarding the reaction mechanism for the formation of Celsian, for the case of the $BaAl_2Si_2O_8$ nominal composition studied, TGA/DTA

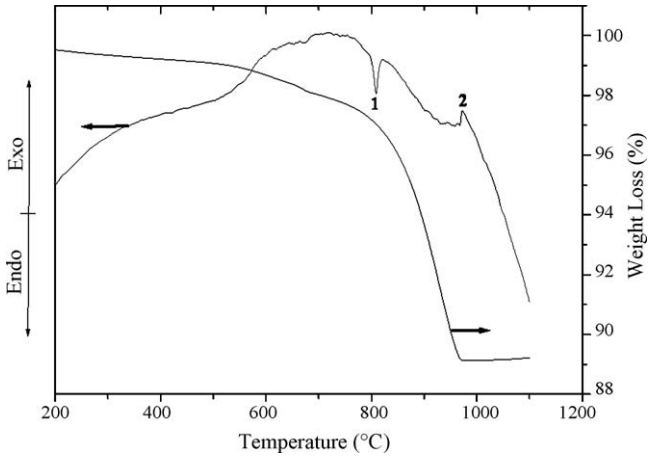


Fig. 4. TGA/DTA curves obtained for a green powder mixture with the $BAS_2$ nominal composition.

analysis was carried out for the corresponding green powder mixture. Fig. 4 shows the results obtained. A weight loss of ~9% occurring in the TGA curve, in the temperature range of ~675–970 °C, can be attributed to the decomposition of $BaCO_3$, for which a theoretical weight loss of 9.82% was expected. An endothermic effect observed in the DTA curve, which has a minimum value at ~808 °C (point 1), can be attributed to two different phenomena occurring at very close temperatures: (a) Whiterite ($BaCO_3$) $\alpha \leftrightarrows \beta$ polymorphic transformation, and (b) decomposition of $BaCO_3$. The exothermic peak at 972 °C (point 2) was attributed to crystallization of Hexacelsian. Moya and Verduch [28] obtained similar results for $BaCO_3$ reacting with kaolin. Since it has been reported [29] that thermal decomposition of pure $BaCO_3$ ends at a temperature of 1360 °C, thus, the final decomposition temperature of ~970 °C determined from the TGA curve was probably associated with the chemical interaction of this carbonate with other components present in the mixture, particularly $SiO_2$, amorphous phases and mullite, at a relatively low temperature, rather than with its thermal decomposition. This is supported by the fact that the presence of BaO was not detected by XRD for any of the compositions and treatment temperatures studied.

Maitra and Foger [30] reported that $BaCO_3$ interacts strongly and irreversibly with $SiO_2$, forming various barium silicates. These authors found, in derivative TG (DTG) plots that for Ba-rich samples there are two regions of decomposition. The first one, located at ~500 °C, corresponds to the formation of barium silicates, while the second one corresponds to the decomposition of $BaCO_3$. The peak temperature for the latter step tends to decrease with increasing $SiO_2$ content. In this way, this temperature decreases from 1100 °C for pure $BaCO_3$ to 1033 °C for a sample with a Ba:Si molar ratio of 3:1. For samples having a Ba:Si molar ratio of either 2:1 or 1:1, the $BaCO_3$ decomposition peak completely disappears and the DTG plot shows only one peak at ~755–780 °C, corresponding to the formation of barium silicates. It is worth mentioning that these authors also reported that when $BaCO_3$ is mixed with $Al_2O_3$, with a Ba:Al molar ratio of 1:2, the DTG plot shows also two peaks, one of which is observed just above 800 °C, corresponding to the formation of barium aluminate, and another one corresponding to the decomposition of $BaCO_3$, located at 140 °C below the peak temperature for the occurrence of the same event in the pure carbonate. They emphasized that, for the case of $BaCO_3$–$Al_2O_3$ mixtures, the decomposition of unreacted carbonate is always the major event, even for samples containing an excess of alumina.

Table 6 shows, in general, that thermal treatment at 850 °C/5 h was sufficient to react all quartz and mullite, as well as a part of the amorphous phase contained in the CFA, with part of the added $Al_2O_3$ and with all the BaO formed by the decomposition of $BaCO_3$, forming various barium silicates and Hexacelsian, without appreciable formation of barium aluminates, which appeared only at temperatures ≥900 °C. Lee and Aswath [16] mentioned that by using aluminum silicates as starting materials, the reaction path leading to the formation of Hexacelsian occurs via the initial formation of barium silicates. In this way, Hexacelsian can be formed at relatively low temperatures. This agrees with the results obtained from the XRD and TGA/DTA analyses carried out in the present work. The use of CFA as main raw material, which contains $Al_2O_3$ and $SiO_2$ already chemically combined forming mullite and amorphous phases, as well as a large amount of free $SiO_2$ (quartz), facilitated the occurrence of solid-state reactions leading to the initial formation of transient barium silicates instead of barium aluminate, and this in turn led to an easy formation of Hexacelsian, which was subsequently relatively easily transformed into Celsian.

From the XRD and TGA/DTA results obtained, it was deduced that, for the case of the $BaAl_2Si_2O_8$ nominal composition studied, the likely reaction path was as follows:

(a) The reaction between $BaCO_3$ and silica starts at $T > 850$ °C through a series of exothermic reactions. The formation of Ba-silicates as transient phases can be produced by reactions (1)–(6). Reaction (2) has the lowest Gibbs free energy and therefore is the most viable. However, as it is obvious, this reaction does not happen until BaO is available once $BaCO_3$ decomposes.

$$BaCO_3 + SiO_2 = BaSiO_3 + CO_2, \quad \Delta G^{900\,^\circ C} = -19.61\,\text{kcal} \tag{1}$$

$$2BaCO_3 + SiO_2 = Ba_2SiO_4 + 2CO_2(g), \quad \Delta G^{900\,^\circ C} = -31.12\,\text{kcal} \tag{2}$$

$$BaCO_3 + 2SiO_2 = BaSi_2O_5 + CO_2(g), \quad \Delta G^{900\,^\circ C} = -23.5\,\text{kcal} \tag{3}$$

$$BaSiO_3 + BaCO_3 = Ba_2SiO_4 + CO_2(g), \quad \Delta G^{900\,^\circ C} = -5.35\,\text{kcal} \tag{4}$$

$$2BaSiO_3 + SiO_2 = Ba_2Si_3O_8, \quad \Delta G^{900\,^\circ C} = -5.82\,\text{kcal} \tag{5}$$

$$Ba_2Si_3O_8 + SiO_2 = 2BaSi_2O_5, \quad \Delta G^{900\,^\circ C} = -1.85\,\text{kcal} \quad (6)$$

The presence of barium silicates ($Ba_2SiO_4$, $BaSiO_3$ and $BaSi_2O_5$) was detected by XRD after thermal treatment of the samples in the temperature range of 850–1000 °C, so a fast reaction between BaO/$BaCO_3$ and $SiO_2$ for the formation of barium silicates was assumed to occur at these temperatures. Indeed, other researchers [31,32] have stated that $BaSiO_3$ is the first barium silicate to form. $BaSiO_3$ led later on to the formation of both $Ba_2SiO_4$ (reaction (4)) and $BaSi_2O_5$ (reaction (6)) barium silicates, during holding time at this temperature. All quartz contained in the CFA was consumed mainly for the formation of barium silicates (reactions (1)–(3), (5) and (6)). It is worth mentioning that formation of $BaSi_2O_5$ directly from $BaSiO_3$ has not been reported in the literature, thus, although the intermediate $Ba_2Si_3O_8$ barium silicate could be formed [31], probably this compound was not detected by XRD due to a fast rate for reactions (5) and (6).

(b) Formation of Hexacelsian in the temperature interval 850–1100 °C as a metastable phase can take place by the following reactions:

$$Al_6Si_2O_{13} + 3BaCO_3 + 4SiO_2 = 3BaAl_2Si_2O_8 + 3CO_2, \quad \Delta G^{900\,^\circ C} = -103.49\,\text{kcal} \quad (7)$$

$$BaSi_2O_5 + Al_2O_3 = BaAl_2Si_2O_8, \quad \Delta G^{900\,^\circ C} = -12.05\,\text{kcal} \quad (8)$$

Thermodynamic calculations indicate that reaction (7) has the lowest Gibbs free energy; hence, it is the most favourable. Similarly, the amorphous phase contained in the CFA was consumed for the formation of Hexacelsian (reaction (9)):

$$[mSiO_2{\cdot}nAl_2O_3]_{\text{Amorphous}} + (m/2{-}n)Al_2O_3 + (m/2)BaCO_3 = (m/2)BaAl_2Si_2O_8 + (m/2)CO_2 \quad (9)$$

Due to a lack of thermodynamic data for the amorphous phase contained in the CFA, the Gibbs free energy of reaction (9) could not be calculated. However, since such an amorphous phase is considered to be highly reactive, it is very likely that reaction (9) was thermodynamically favourable.

(c) Between 900 and 1100 °C formation of Hexacelsian continued via reaction (8), with additional amounts of this phase formed at the expense of the remaining $Al_2O_3$ and some of the barium silicates previously formed (reaction (10)):

$$BaSi_2O_5 + Al_2O_3 = BaAl_2Si_2O_8, \quad \Delta G^{1100\,^\circ C} = -12.6\,\text{kcal} \quad (10)$$

(d) The formation of $BaAl_2O_4$ by reaction of previously formed barium silicates or by direct reaction of $Al_2O_3$ with $BaCO_3$ or BaO is not thermodynamically viable (reactions (11)–(13)). Thus, the formation of barium aluminates was probably due to the presence of areas enriched in aluminum and barium in the sample.

$$2BaSiO_3 + Al_2O_3 = BaAl_2Si_2O_8 + BaAl_2O_4, \quad \Delta G^{900\,^\circ C} = +38.6\,\text{kcal} \quad (11)$$

$$Ba_2SiO_4 + Al_2O_3 = BaAl_2O_4 + BaSiO_3, \quad \Delta G^{1100\,^\circ C} = +40.1\,\text{kcal} \quad (12)$$

$$BaCO_3 + Al_2O_3 = BaAl_2O_4 + CO_2(g), \quad \Delta G^{900\,^\circ C} = +24.6\,\text{kcal} \quad (13)$$

$$BaO + Al_2O_3 = BaAl_2O_4, \quad \Delta G^{900\,^\circ C} = +5.6\,\text{kcal} \quad (14)$$

Lee and Aswath [16] mentioned that once $BaAl_2O_4$ is formed, this compound tends to remain even after thermal treatment at 1530 °C/50 h, due to a pretty low reaction rate of $BaAl_2O_4$ with $SiO_2$ to form Hexacelsian. In this work, traces of barium aluminates were detected on the SEM but not by XRD in samples heat treated at 1300 °C, probably because at this temperature the content of barium aluminates was below the detection limit of the XRD technique employed. This sample shows a homogeneous microstructure with randomly distributed clusters of Ba-aluminates. No diffusion or reaction within the clusters and the rest of the sample occurred probably because the coarse Ba-aluminates were in equilibrium at local level with Celsian, and thus, it was not possible to eliminate them by heat treatment. However, most of the $BaAl_2O_4$ formed by the mechanism explained above was slowly consumed by reaction (15) in the temperature range of 900–1300 °C, involving the participation of free crystalline quartz and $SiO_2$ contained in the glassy phase, both of them present in the CFA.

$$BaAl_2O_4 + SiO_2 = BaAl_2Si_2O_8, \quad \Delta G^{900\,^\circ C} = -60.08\,\text{kcal} \quad (15)$$

At ~1300 °C the last $BaSi_2O_5$ remaining could be also completely consumed by $Al_2O_3$ contained in the remnant glassy phase of the CFA, according to reaction (8).

(e) Lastly, between 1100 and 1300 °C, the Hexacelsian to Celsian conversion continued, in such a way that the latter phase became predominant at 1200 °C. It is worth mentioning that small deviations from the Celsian stoichiometry within the samples could induce the development of small quantities of transitory liquid phases in the vicinity of the eutectic point of the subsystem $BaAl_2Si_2O_8$–$BaSi_2O_5$–$SiO_2$ at 1122 °C [33]. These liquid phases could also enhance the polymorphic transformation of Hexacelsian to Celsian. However, this effect was considered to be small and it was not evaluated.

In the case of the SrO-doped compositions studied, a reaction mechanism similar to that proposed above was probably followed for the formation of $Ba_{1-x}Sr_xAl_2Si_2O_8$

solid solutions with monoclinic structure, i.e., the formation of the same phases took place following a similar sequence for all nominal compositions studied, with or without SrO doping, except for the case of the B2S7 material, for which strontium silicates and aluminate were formed instead of the corresponding barium compounds. This suggests that, at relatively low SrO concentrations, this oxide participated predominantly in the formation of $Ba_{1-x}Sr_xAl_2Si_2O_8$ solid solutions, instead of reacting with $SiO_2$ and/or $Al_2O_3$ for the formation of strontium silicates and/or strontium aluminate. However, at SrO levels of $0.75 \leq x \leq 1$, the formation of the latter compounds predominated, at all treatment temperatures employed. Krzmanc et al. [25] obtained similar results for SrO concentrations in the range of $0.6 \leq x \leq 1$.

The most important difference observed between the undoped and SrO-doped Celsian compositions was that in the latter case all reactions started at lower temperatures. In this case, the Hexacelsian to Celsian conversion started in the temperature range of 900–1000 °C, with an increased proportion of the latter phase with increasing SrO content at 1000 °C. The proportion of Celsian also increased with increasing temperature for a given SrO level, becoming the predominant phase at 1100 °C. At 1200 °C, all the SrO-doped materials were composed entirely of Celsian, except for the B2S7 nominal composition, which contained additional traces of strontium aluminate.

In the case of the $SrAl_2Si_2O_8$ composition, a reaction mechanism similar to that deduced for the $BaAl_2Si_2O_8$ material was also followed, although in the case of the first composition the mullite present in the CFA completely disappeared only at 900 °C, probably due to reactions (16) and (17):

$$Al_6Si_2O_{13} + 3SrCO_3 + 4SiO_2 = 3SrAl_2Si_2O_8 + 3CO_2, \quad \Delta G^{900\,^\circ C} = -103.5\,\text{kcal} \tag{16}$$

$$Al_6Si_2O_{13} + 2SrSiO_3 = 2SrAl_2Si_2O_8 + Al_2O_3, \quad \Delta G^{900\,^\circ C} = -27.6\,\text{kcal} \tag{17}$$

The formation of metastable Sr-silicates ($SrSiO_3$, $Sr_2SiO_4$) was detected by XRD at 900 °C (reactions (18) and (19)):

$$SrCO_3 + SiO_2 = SrSiO_3 + CO_2(g), \quad \Delta G^{900\,^\circ C} = -20.8\,\text{kcal} \tag{18}$$

$$2SrCO_3 + SiO_2 = Sr_2SiO_4 + 2CO_2(g), \quad \Delta G^{900\,^\circ C} = -30.9\,\text{kcal} \tag{19}$$

Another difference observed with respect to the $BaAl_2Si_2O_8$ material was the formation of a strontium aluminosilicate ($Sr_2Al_2SiO_7$, $s_2AS$), different in chemical composition to Celsian SAS, additionally to the formation of strontium silicates, strontium aluminate and Hexacelsian occurring at 900 °C (reactions (20)–(24)). $Sr_2Al_2SiO_7$ disappeared later on at 1200 °C.

$$SrO + Al_2O_3 = SrAl_2O_4 \tag{20}$$

$$Sr_2SiO_4 + Al_2O_3 = Sr_2Al_2SiO_7 \tag{21}$$

$$Sr_2SiO_4 + Al_2O_3 = SrAl_2O_4 + SrSiO_3 \tag{22}$$

$$SrSi_2O_5 + Al_2O_3 = SrAl_2Si_2O_8 \tag{23}$$

$$2SrSiO_3 + 2Al_2O_3 = SrAl_2Si_2O_8 + SrAl_2O_4 \tag{24}$$

The Gibbs free energy of reactions (20)–(24) could not be calculated due to a lack of thermodynamic data for some of the chemical species involved in them. However, since the formation of all their chemical products were indeed detected by XRD, it can be safely assumed that all of these reactions are thermodynamically favourable at temperatures ≥900 °C.

Lastly, Celsian SAS was the predominant phase at 1300 °C, with the presence of only trace amounts of Hexacelsian and strontium aluminate at this temperature.

Although the proposed reaction mechanism can help us to explain the evolution of phases observed in our materials as a function of treatment temperature, it is worth mentioning that there is also a likely mineralizing effect caused by some of the impurities present in the CFA, particularly CaO and $TiO_2$ [12], which could promote an easy stabilization of Celsian at a relatively low temperature. This will be discussed further in the following section.

### *3.4. Mineralizing effect of some impurities present in the CFA on the stabilization of Celsian*

Besides the SrO dopant added in order to promote the Hexacelsian to Celsian transformation, many of the impurities contained in the CFA, namely $Na_2O$, CaO, $TiO_2$, MgO and $K_2O$, Table 4, are also known to greatly enhance the kinetics of this conversion. Among these oxides, CaO and $TiO_2$ are the most important ones in terms of their concentration and mineralizing effect in the materials synthesized in this work.

According to Lee and Aswath [12], both CaO and $TiO_2$ are more efficient mineralizers than $SrF_2$. These authors established that the minimum treatment temperature required for full conversion of Hexacelsian into Celsian, for a constant dopant addition of 10 mol.%, is: ∼1200 °C for CaO, ∼1250 °C for $TiO_2$, and ∼1300 °C for $SrF_2$. On the other hand, the minimum dopant amount required to achieve full conversion at 1250 °C/4 h, is: ∼2 mol. % for either CaO or $TiO_2$, and ∼12 mol. % for $SrF_2$. The minimum concentration of 2 mol.% is equivalent either to 0.3 wt.% of CaO or to 0.43 wt.% of $TiO_2$. Table 5 shows that in our materials the CaO concentration varied from 1.31 to 1.62 wt.%, while that of $TiO_2$ varied from 0.45 to 0.61 wt.%. This means that all synthesized materials had a concentration of both impurities above the minimum values required for full stabilization of Celsian, according to Ref. [12]. Thus, in this work, a synergistic mineralizing effect of CaO and $TiO_2$ present in the CFA, which acted in combination with the SrO dopant added, could account for the observed stabilization of Celsian at relatively low temperatures. This is supported by the SEM/EDS results obtained, which are given in Fig. 5 and Table 7. Points 2 and 3 indicated in the micrographs of Fig. 5 correspond to Celsian ($BaAl_2Si_2O_8$) grains containing $Fe_2O_3$, CaO, $Na_2O$ and $TiO_2$ as impurities, according to Table 7. On the other hand, points 1 and 4 correspond to elongated needle-like

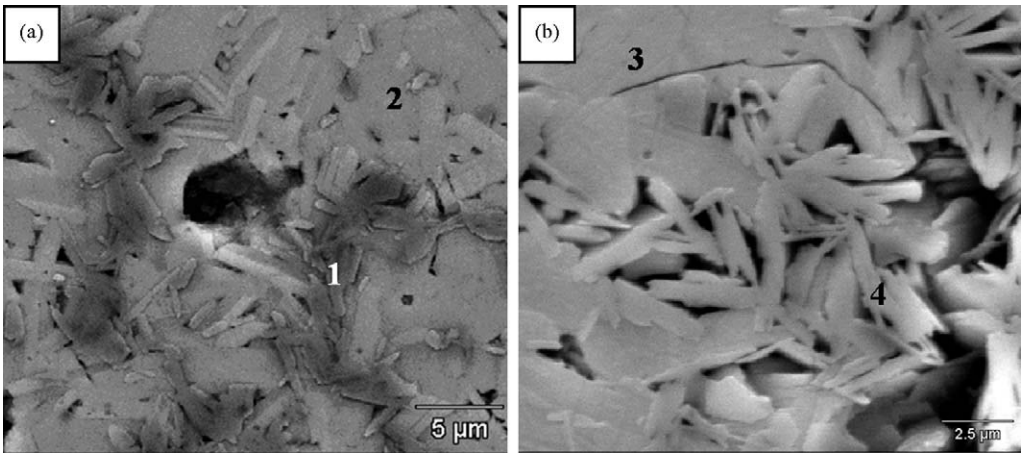


Fig. 5. SEM micrographs of HF-etched $BAS_2$ specimens heat treated at 1300 °C/5 h. (a) Backscattered electrons image, (b) secondary electrons image.

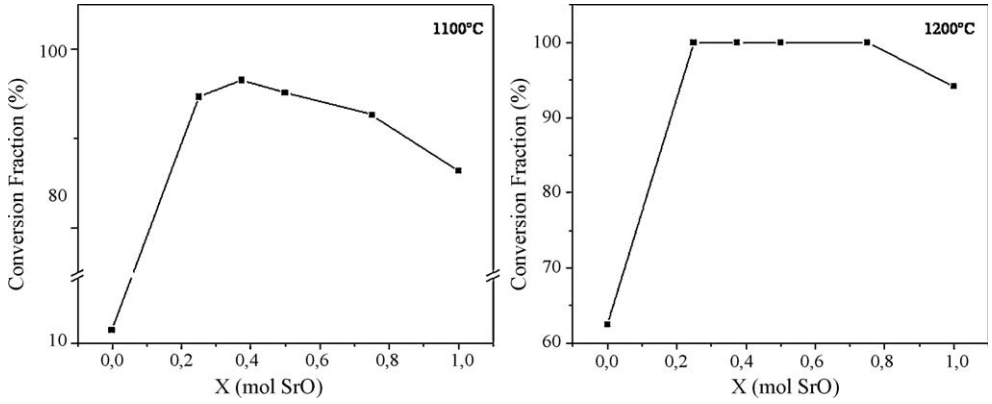


Fig. 6. Hexacelsian to Celsian conversion fraction as a function of SrO added, after heat treatment at 1100 or 1200 °C for 5 h.

barium aluminate grains, which contained $Fe_2O_3$, MgO and $K_2O$ as impurities. Thus, the CFA impurities known to have a strong mineralizing effect on the Hexacelsian to Celsian transformation tended to concentrate in the phase with nominal chemical composition of $Ba_{1-x}Sr_xAl_2Si_2O_8$.

Lee and Aswath [12] mentioned that the addition of mineralizers induces the generation of oxygen and barium vacancies in Hexacelsian, by assisting the braking of its Ba–O or (Al,Si)–O bonds, and thus promoting in this way its transformation into Celsian. In the case of mineralizers with cationic radii of ~0.99 Å, such as CaO, this transformation is likely promoted by formation of an interstitial solid solution in which the $Ca^{2+}$ cations reside in the double six-ring (D6R) sites of the hexagonal cell, with the consequent creation of $Ba^{2+}$ vacancies, according to the reaction:

$$CaO = Ca_i^{oo} + V_{Ba}^{''} + O_O^X + V^X \quad (25)$$

It has also been mentioned [34] that the addition of CaO enhances the Hexacelsian to Celsian transformation by promoting the formation of Celsian nuclei with a plate-like morphology on the basal planes of the Hexacelsian structure.

In the case of mineralizers with cationic radii of ~0.66 Å, such as $TiO_2$, the Hexacelsian to Celsian transformation is likely promoted by substitution of the host $Al^{3+}$ (or $Si^{4+}$) ions by the guest $Ti^{4+}$ ions, also with a consequent creation of $Ba^{2+}$ vacancies, according to the reaction:

$$2TiO_2 = 2TiAl^o + V_{Ba}^{''} + 4O_O^X + 2V^X \quad (26)$$

Lastly, for the case of SrO-doped materials, Lee and Aswath [12] mentioned that the $Sr^{2+}$ ions could reside in both the $Ba^{2+}$-host sites and the D6R interstitial sites of Hexacelsian. However, the fact that $Ca^{2+}$ is a much more efficient dopant than $Sr^{2+}$ [34], could indicate that the $Sr^{2+}$ ions reside mainly in the $Ba^{2+}$-host sites of Hexacelsian.

Table 7
Results of SEM/EDS analyses (wt.%) carried out in $BAS_2$ specimens of Fig. 5.

| Analyzed point | $SiO_2$ | $Al_2O_3$ | BaO | $Fe_2O_3$ | CaO | $Na_2O$ | $K_2O$ | MgO | $TiO_2$ |
|---|---|---|---|---|---|---|---|---|---|
| 1 | 2.41 | 55.74 | 30.26 | 2.69 | | 1.16 | 2.47 | 3.31 | 1.97 |
| 2 | 28.8 | 19.59 | 46.78 | 1.17 | | 0.75 | | | 2.91 |
| 3 | 30.0 | 21.82 | 46.97 | 0.66 | 0.55 | | | | |
| 4 | 2.97 | 64.74 | 16.43 | 9.91 | 0.88 | | 2.4 | 2.66 | |

### 3.5. Hexacelsian to Celsian conversion fraction

According to Fig. 6, a maximum Hexacelsian to Celsian conversion fraction of ∼96% was achieved for $x = 0.375$ at 1100 °C/5 h, while full conversion was achieved by doping the $BaAl_2Si_2O_8$ composition with SrO in the range of $0.25 \leq x \leq 0.75$ at 1200 °C/5 h. As already mentioned, these conversion levels are much higher than those reported by Fu et al. [17], who achieved a maximum conversion of ∼40% for $x = 0.375$, after calcination at 950 °C/4 h followed by heat treatment at 1040 °C/4 h. For the case of undoped $BaAl_2Si_2O_8$, it can be seen that the conversion fraction is increased from ∼12 to ∼62% by increasing temperature from 1100 to 1200 °C.

These results show that the optimum conditions to achieve full Hexacelsian to Celsian conversion appear to involve the addition of a suitable amount of $SrCO_3$ to the initial mixture of CFA, $Al_2O_3$, $SiO_2$ and $BaCO_3$ employed in the present work, in order to have a SrO concentration in the range of $0.25 \leq x \leq 0.75$ in the materials thermally treated at 1200 °C/5 h. However, the most recommended addition level within the mentioned range will ultimately depend on how it influences other properties of the materials, such as liquidus temperature and thermal expansion coefficient, which are two of the most important properties when structural applications at high temperature are envisaged. Bansal et al. [13] reported only a small variation in both properties as a function of SrO content, for SrO-containing $BaAl_2Si_2O_8$ glasses. However, Fu et al. [17] found, for materials synthesized by the solid-state reaction route, that the average thermal expansion coefficient decreased with increasing SrO content, from $\sim 16\ x\ 10^{-6}/°C$ for $BaAl_2Si_2O_8$ with no added SrO, to a minimum value of $\sim 7\ x\ 10^{-6}/°C$ for SrO concentrations of $0.25 \leq x \leq 0.475$, in the temperature range of 25–400 °C. These authors recommended an optimum SrO addition level of $x = 0.375$. Based on these results, as well as on those obtained in the present work, the optimum SrO level recommended by us is $0.25 \leq x \leq 0.375$.

### 3.6. Rietveld refinement of synthesized materials

Before starting the Rietveld refinements, the instrumental broadening of the diffractometer was determined with the aid of a $LaB_6$ NIST standard with a known narrow crystallite size distribution. The peak shape model employed was the one of Thompson–Cox–Hastings (TCA). For asymmetry corrections, the model of Bérar–Baldinozzi [35] was employed. The background was fitted to a 20 degree polynomial. With these premises, the Pawley refinements were initiated setting free the zero shift of the goniometer $2\theta^\circ$ scale, asymmetry, crystallite size, lattice strain, cell parameters and background coefficients. The Cagliotti coefficients $(u, v, w)$, and $X$ and $Y$ coordinates of the TCA peak shape were always kept constant since they determine the instrumental broadening. After a few cycles, the refinements converged. In a second stage, the Rietveld refinements were initiated using as starting values the ones found in the first stage. The occupancy of large Ba/Sr cations were first set free, on top of the parameters refined by the Pawley method [36], doing then the same with the atomic positional parameters, the preferential orientation parameters according to the model of Rietveld-Toraya [37], and, finally, the global isotropic Debye–Waller factor. The statistics of the diffraction pattern due to the presence of other phases and the limitations of the instrument did not allow the determination of individual isotropic Debye–Waller factors. When attempted, some of the ionic species attained meaningless physical values. The rest of the refined parameters reached acceptable values, including the atomic coordinates of all ion species.

Table 8
Agreement factor, cell parameters (Å) and occupancies after the Rietveld refinements. The errors of cell parameters are ±0.004. The errors associated to the occupancy are ±0.03.

| Sample code | $R_{wp}$ | $a$ | $b$ | $c$ | $\beta$ | Ba occ. |
|---|---|---|---|---|---|---|
| $BAS_2$ | 7.82 | 8.636 | 13.054 | 7.205 | 115.040 | 0.938 |
| B7S2 | 6.60 | 8.581 | 13.039 | 7.190 | 115.088 | 0.853 |
| B6S3 | 5.67 | 8.543 | 13.011 | 7.171 | 115.103 | 0.827 |
| B5S5 | 5.59 | 8.516 | 13.009 | 7.166 | 115.134 | 0.792 |
| B2S7 | 6.07 | 8.444 | 12.986 | 7.143 | 115.196 | 0.708 |
| SAS | 7.81 | 8.374 | 12.955 | 7.119 | 115.302 | 0.616 |

Table 9
Crystallographic data for the studied compositions, according to the corresponding JCPDS cards [38].

| Sample code | $a$ | $b$ | $c$ | $\beta$ |
|---|---|---|---|---|
| $BAS_2$ | 8.641 | 13.04 | 7.203 | 115.07 |
| B7S2 | 8.58 | 1.303 | 7.189 | 115.15 |
| B5S5 | 8.51 | 13.01 | 7.169 | 115.13 |
| B2S7 | 8.45 | 12.99 | 7.151 | 115.23 |
| SAS | 8.393 | 12.97 | 7.132 | 115.38 |

The most relevant parameters found after the Rietveld refinements are shown in Table 8. All cell parameters are very similar to those reported in the JCPDS cards [38] for $SrAl_2Si_2O_8$ and $BaAl_2Si_2O_8$ (with and without Sr content), as shown in Table 9. This implies that the materials synthesized in the present work were chemically and structurally similar to those obtained from reagent-grade raw materials, whose cell parameters are reported in the JCPDS cards.

Some minor amounts of Ti and Fe were present in the analyzed samples, most likely as $Ti^{4+}$ and $Fe^{3+}$ partially substituting the small $Al^{3+}$ and $Si^{4+}$ ions. Since X-rays do not allow to discriminate between ionic species such as $Si^{4+}$, $Al^{3+}$, $Fe^{+3}$ and $Ti^{4+}$, it was assumed as a good approximation that the population of $Ba^{2+}$ found for Celsian without Sr could be used to determine the small $M^{3+}/M^{4+}$ cation ratio, simply from a balance of charges. For the rest of the Celsian samples, it was supposed that the $M^{3+}/M^{4+}$ ratio was the same and therefore the number of vacancies at that site was considered to be constant. With this hypothesis in mind, the Ba/Sr proportions were estimated for the whole series.

For the occupancy analysis of large cations in site 4(i) only Ba ions were considered, since the Rietveld module of MS4 does not allow the presence of two different species in the same site. To calculate the Ba/Sr ratio for the Sr-containing specimens, the scattering factors for $Ba^{2+}$ and $Sr^{2+}$ were

Table 10
Proportion of barium in the specimens as a function of the refined occupancy ($p$).

| $p$ | 0.938 | 0.853 | 0.827 | 0.792 | 0.708 | 0.616 |
|---|---|---|---|---|---|---|
| $z/(x+z)$ | 1.0 | 0.73 | 0.64 | 0.53 | 0.26 | −0.03 |

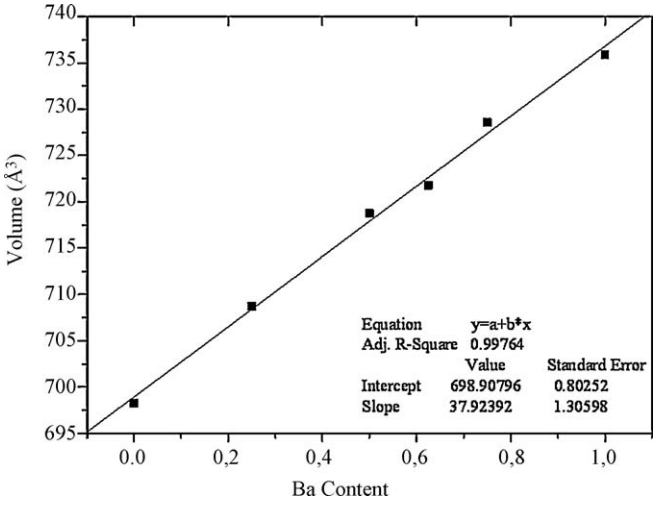


Fig. 7. Variation of cell volume of Celsian samples analyzed as a function of Ba content. A straight line was fitted and its statistic parameters are shown as an inset.

simply considered to be proportional to their respective number of electrons ($Z-2$). Although this is not a completely rigorous assumption, it is a good approximation, bearing in mind the precision of the results attained. In this part of the work, the general formula for the synthesized materials was considered to be $Ba_zSr_x(Al_{1-y},Si_y)_4O_8$, where $z=1-x$ and $y \sim 0.53$, according to the literature. Therefore, the expression governing the proportion of Ba present in every analyzed specimen can be written as:

$$\frac{z}{x+z} = \frac{(z_{BA}-1)(p/0.938)-z_{Sr}-2}{z_{BA}-z_{Sr}} = \frac{3p}{0.938}-2$$

$p$ is the occupancy found for Ba in the Rietveld refinement for the specimen without Sr. A summary of the proportions found can be seen in Table 10.

The theoretical Ba/Sr ratios for the analyzed samples are: 1:0; 0.75:0.25; 0.625:0.375; 0.5:0.5; 0.25:0.75 and 0:1. Thus, Table 10 shows that the calculated proportions of Ba agree very well with the expected values.

The direct approach of finding the Ba/Sr occupancy was tested vs. the more indirect one of correlation with the crystal cell size. Indeed, if the content of small cations in sites T1 and T2 remains constant, the cell parameters should vary in a linear fashion as a function of Ba or Sr content. In Fig. 7, the trend of cell variation can be appreciated. The cell volume has been plotted against Ba content. The linear increase of the cell volume with composition, from $SrAl_2Si_2O_8$ to $BaAl_2Si_2O_8$, indicates that Vegard's rule is obeyed. These results also confirm the formation of $Ba_{1-x}Sr_xAl_2Si_2O_8$ solid solutions over the entire concentration range $0 \le x \le 1$ [24].

## 4. Conclusions

Monoclinic (Celsian) and hexagonal (Hexacelsian) $Ba_{1-x}Sr_xAl_2Si_2O_8$ solid solutions were synthesized by using Coal Fly Ash (CFA) as main raw material, employing a simple one-step solid-state reaction process. The $Ba_{0.625}Sr_{0.375}Al_2Si_2O_8$ composition showed the largest Hexacelsian to Celsian conversion (96%) at 1100 °C/5 h, while full conversion was achieved at 1200 °C/5 h for materials with SrO contents in the range of $0.25 \le x \le 0.75$. An optimum SrO level of $0.25 \le x \le 0.375$ was recommended for stabilization of Celsian at the latter temperature, based on the effect of SrO on the liquidus temperature and thermal expansion coefficient of these materials, reported by other researchers. Chemical analyses and Rietveld refinements showed that the synthesized materials were chemically and structurally similar to analogous materials obtained from reagent-grade powders in previously published literature. The easy stabilization of Celsian at a relatively low temperature and short time, when compared to previously published data, can be attributed to the joint contribution of two main factors: (a) presence of $Al_2O_3$ and $SiO_2$, already chemically combined forming mullite and an amorphous phase, together with a large content of free $SiO_2$ in the CFA employed; this resulted in a reaction path leading to the formation of transient barium silicates ($BaSiO_3$, $Ba_2SiO_4$ and $BaSi_2O_5$) in the temperature range of 850–1100 °C; the formation of barium aluminates was also detected at temperatures higher than 900 °C; all of this led in turn to an easy formation of Hexacelsian; (b) a likely synergistic mineralizing effect of impurities present in the CFA, particularly CaO and $TiO_2$, which could act in combination with the added SrO, greatly facilitating the Hexacelsian to Celsian conversion. Lastly, thermodynamics calculations were used to validate the detailed model for the reaction sintering mechanism. It can be appreciated that the theoretical predictions agree with the sequential appearance of phases. Namely, $\Delta G$ computations for the formation of $BaAl_2Si_2O_8$, $BaSiO_3$, $Ba_2SiO_4$, $Ba_2Si_3O_8$, $BaSi_2O_5$ and $BaAl_2O_4$ confirm the much lower $\Delta G$ value for $BaAl_2Si_2O_8$ in the whole range of temperatures considered. Consequently, its appearance as the first phase during reaction is fully justified.

## Acknowledgements

The authors express their gratitude to CONACYT, México, for the financial support provided for the realization of this work (project no. P47257-Y, under the responsibility of J.L.C.), and for a scholarship granted to D.L.G. to carry out his Ph.D. studies at Cinvestav-Saltillo as well as a research stay at Instituto de Cerámica y Vidrio (ICV), Madrid, Spain. The work in Spain was carried out in the frame of project MEC MAT2006-13480 C02-01. The authors wish to acknowledge the assistance of Dra. P. Recio (ICV) in the course of the XRD analyses. Many thanks are also given

to the personnel of the ''José López Portillo'' power plant for supplying the employed CFA.

## References


[1] X.-D. Zhang, K.H. Sandhage, H.L. Fraser, Synthesis of $BaAl_2Si_2O_8$ from solid Ba–Al–$Al_2O_3$–$SiO_2$ precursors. II. TEM analyses of phase evolution, Journal of the American Ceramic Society 81 (11) (1998) 2983–2997.

[2] R.A. McCauley, Polymorphism and dielectric electric properties of Ba- and Sr-containing feldspars, Journal of Materials Science 35 (15) (2000) 3939–3942.

[3] J.S. Moya Corral, G. Verduch, The solid solution of silica in celsian, Transactions and Journal of the British Ceramic Society 77 (2) (1978) 40–44.

[4] V.S.R. Murthy, M.H. Lewis, Matrix crystallization and interface structure in SiC-Celsian composites, Transactions and Journal of the British Ceramic Society 89 (5) (1990) 173–174.

[5] N.P. Bansal, Strong and tough Hi-Nicalon-fiber-reinforced celsian matrix composites, Journal of the American Ceramic Society 80 (9) (1997) 2407–2409.

[6] K.N. Lee, D.S. Fox, J.I. Eldridge, D. Zhu, R.C. Robinson, N.P. Bansal, R.A. Miller, Upper temperature limit of environmental barrier coatings based on mullite and BSAS, Journal of the American Ceramic Society 86 (8) (2003) 1299–1306.

[7] B. Yoshiki, K. Matsumoto, High-temperature modification of barium feldspar, Journal of the American Ceramic Society 80 (9) (1997) 2021–2029.

[8] H.C. Lin, W.R. Foster, Studies in the system $BaO{\cdot}Al_2O_3{\cdot}SiO_2$. I. The polymorphism of celsian, American Mineralogist 53 (1–2) (1968) 134–144.

[9] N. Frety, A. Taylor, M.H. Lewis, Microstructure and crystallization behavior of sol–gel derived 1/2SrO–1/2BaO–$Al_2O_3$–$2SiO_2$ glass–ceramic, Journal of Non-Crystalline Solids 195 (1–2) (1996) 28–37.

[10] Y. Kobayashi, Transformation kinetics from hexacelsian to celsian for powders having uniform particle size, Ceramics International 27 (2) (2001) 179–184.

[11] M.C. Guillem Villar, C. Guillem Monzonis, J.A. Navarro, Reactions between kaolin and barium carbonate: influence of mineralizers. 1. Qualitative study, Transactions and Journal of the British Ceramic Society 82 (2) (1983) 69–72.

[12] K.T. Lee, P.B. Aswath, Role of mineralizers on the hexacelsian to celsian transformation in the barium aluminosilicate ($BAS_2$) system, Materials Science and Engineering A 352 (1–2) (2003) 1–7.

[13] N.P. Bansal, M.J. Hyatt, C.H. Drummond III, Crystallization and properties of Sr–Ba aluminosilicate glass–ceramic matrices, Ceramic Engineering and Science Proceedings 12 (7–8) (1991) 1222–1234.

[14] S.S. Amritphale, A. Anshul, N. Chandra, N. Ramakrishnan, Development of celsian ceramics from fly ash useful for X-ray radiation-shielding application, Journal of the European Ceramic Society 27 (16) (2007) 4639–4647.

[15] L.D. Hulett, A.J. Weinberger, K.J. Northcutt, M. Fergusone, Chemical species in fly ash from coal-burning power plant, Science 210 (4476) (1980) 1356–1358.

[16] K.-T. Lee, P.B. Aswath, Enhanced production of celsian barium aluminosilicates by a three-step firing technique, Materials Chemistry and Physics 71 (1) (2001) 47–52.

[17] Y.-P. Fu, C.-C. Chang, C.-H. Lin, T.-S. Chin, Solid-state synthesis of ceramics in the BaO–SrO–$Al_2O_3$–$SiO_2$ system, Ceramics International 30 (1) (2004) 41–45.

[18] Accelrys Materials Studio v. 40, Accelrys, Cambridge, CB4 OWN, UK, 2005.

[19] M.G. Skellern, R.A. Howie, E.E. Lachowski, J.M.S. Skakle, Barium-deficient celsian, $Ba_{1-x}Al_{2-2x}Si_{2+2x}O_8$ ($x = 0.20$ or 0.06), Acta Crystallographica Section C: Crystal Structure Communications 59 (2) (2003) i11–i14.

[20] Outokumpu Research Oy, Pori, Finland Outokumpu HSC Chemistry for Windows Version 1.10, 1993.

[21] S. Gomes, M. Francois, Characterization of mullite in silicoaluminous fly ash by XRD, TEM, and Si MAS NMR, Cement and Concrete Research 30 (2) (2000) 175–181.

[22] L.D Hulett, A.J. Weinberger, Some etching studies of the microstructure and composition of large aluminosilicate particles in fly ash from coal-burning power plants, Environmental Science and Technology 14 (8) (1980) 965–970.

[23] I.G. Talmy, D.A. Haught, Celsian-based ($BaO{\cdot}Al_2O_3{\cdot}SiO_2$) ceramics as candidates for radomes, in: Proceedings of the 14th Conference on Metal, Carbon and Ceramic Composites, NASA Conference Publication No. 3097, Part I, 1990, pp. 227–238.

[24] N.P. Bansal, Solid state synthesis and properties of monoclinic celsian, Journal of Materials Science 33 (19) (1998) 4711–4715.

[25] M.M. Krzmanc, M. Valant, D. Suvorov, The synthesis and microwave dielectric properties of $Sr_xBa_{1-x}Al_2Si_2O_8$ and $Ca_yBa_{1-y}Al_2Si_2O_8$ ceramics, Journal of the European Ceramic Society 27 (2–3) (2007) 1181–1185.

[26] N.P. Bansal, Celsian formation in fiber-reinforced barium aluminosilicate glass–ceramic matrix composites, Materials Science and Engineering A 342 (1–2) (2003) 23–27.

[27] Y. Kobayashi, M. Inagaki, Preparation of reactive Sr-celsian powders by solid-state reaction and their sintering, Journal of the European Ceramic Society 24 (2) (2004) 399–404.

[28] J.S. Moya, G. Verduch, Estudio de la reacción entre el caolín y el carbonato de bario, Boletín de la Sociedad Española de Cerámica y Vidrio 15 (6) (1976) 379–381.

[29] I. Arvanitidis, D. Sichen, S. Seetharaman, A study of the thermal decomposition of $BaCO_3$, Metallurgical and Materials Transactions B 27 (3) (1996) 409–416.

[30] A.M. Maitra, K. Foger, Identification of solid solutions and other phases in strontium and barium catalysts containing oxides of magnesium, aluminum or silicon as additive. II. Catalyst characterization, Applied Catalysis A: General 114 (1) (1994) 83–107.

[31] K.-T. Lee, P.B. Aswath, Synthesis of hexacelsian barium aluminosilicate by a solid-state process, Journal of the American Ceramic Society 83 (12) (2000) 2907–2912.

[32] A. Bandyopadhyay, P.B. Aswath, A phase transformation study in the $BaO{\cdot}Al_2O_3{\cdot}SiO_2$ (BAS)–$Si_3N_4$ system, Journal of Materials Research 10 (12) (1995) 3143–3148.

[33] E.M. Levin, H.F. McMurdie, Phase Diagram for Ceramists, vol. 3, The American Ceramic Society, Westerville, OH, 1975, p. 220.

[34] K.-T. Lee, P.B. Aswath, Kinetics of the hexacelsian to celsian transformation in barium aluminosilicates doped with CaO, International Journal of Inorganic Materials 3 (7) (2001) 687–692.

[35] J. Baldinozzi, J.F. Bérar, Modeling of line-shape asymmetry in powder diffraction, Journal of Applied Crystallography 26 (1) (1993) 128–134.

[36] G.S. Pawley, Unit-cell refinement from powder diffraction scans, Journal of Applied Crystallography 14 (6) (1981) 357–361.

[37] H. Toraya, F. Marumo, Preferred orientation correction in powder pattern-fitting, Mineralogical Journal 10 (5) (1981) 211–221.

[38] JCPDS Cards: #381450 for monoclinic $BaAl_2Si_2O_8$, # 381451 for $Ba_{0.75}Sr_{0.25}Al_2Si_2O_8$, # 381452 for $Ba_{0.5}Sr_{0.5}Al_2Si_2O_8$, # 381453 for $Ba_{0.25}Sr_{0.75}Al_2Si_2O_8$, # 381454 for $SrAl_2Si_2O_8$.